Isentropic correction for collocated Lagrange-Remap scheme

C. Paulin, J.-P. Braeunig, R. Motte

Version of Record: https://www.sciencedirect.com/science/article/pii/S0898122118303638
Manuscript_12061dcdea0b11c4209a76793a156507

Isentropic correction for collocated Lagrange-Remap scheme

C. Paulin[b], J.-P. Braeunig[a,*], R. Motte[a]

[a]*CEA, DAM, DIF, F-91297 Arpajon, France*
[b]*CMLA, ENS Cachan, CNRS, Université Paris-Saclay, and LRC MESO*

Abstract

We study an Eulerian scheme of Lagrange-Remap type, which simulates compressible multi-material fluid flows. The Lagrangian phase is based on a collocated scheme called EUCCLHYD (Explicit Unstructured Cell-Centered Lagrangian HYDrodynamics, [1]), whereas the remap phase uses alternate directions with interface reconstruction of PLIC type. The EUCCLHYD scheme, which is built on the resolution of acoustic Riemann problems at nodes, is totally conservative, second order in time and space, and captures shock waves accurately. However, the intrinsic entropy production is inaccurate for isentropic flows (rarefaction/expansion waves, isentropic compression). In this framework we suggest a correction, inspired by Braeunig, 2016, [2], to improve accuracy in flows with isentropic behavior. This is achieved by modifying the scheme in order to nullify the entropy production in expansion zones.

Keywords: Collocated scheme, Lagrange-Remap, Entropy production, Isentropic flows

1. Introduction

Numerical simulations have widespread applications in physics. The goal of this study is to improve the collocated Lagrangian scheme called EUCCLHYD (Explicit Unstructured Cell-Centered Lagrangian HYDrodynamics, [1]) in order to reduce its numerical dissipation. Collocated means that the velocity or momentum variables of the scheme are cell-centered along with the other thermodynamical variables, in contrast to classical staggered schemes, where velocity or momentum variables are located at nodes or faces, whereas the other variables are cell centered. Robustness of the schemes when refining the mesh may be an important issue in order to perform simulations of higher resolution and resolve more details of the flow. EUCCHLYD is used in numerous applications such as simulations of blast waves or ICF (Inertial Confinement Fusion) for instance. The challenge in modelling these applications is that the numerical scheme needs to be robust, entropy dissipative, conservative, and convergent.

Historically, Godunov[1] presented in his 1959 article [5] a new method to resolve the Euler equations, which is known as the first *Riemann solver*. Godunov invented his famous numerical scheme in order to respond to article [6] of J. Von Neumann and R.D. Richtmyer published in 1950. This article was an inspiration to classical staggered schemes, such as VNR [6], Wilkins [7], and Youngs [8]. These methods have been designed to introduce low dissipation on coarse meshes by writing an internal energy evolution equation based on isentropic hypothesis, but then a so-called *artificial viscosity* is necessary to dissipate energy in discontinuities in accordance to physics and to stabilize the scheme. However, the non-conservative form of these schemes by using internal energy equation is a drawback, since the Lax-Wendroff theorem does not apply and convergence cannot be guaranteed, what is crucial when refining meshes.

The improvement of symmetry preservation, verification of the conservation law and validation of correct solutions is treated in the work of Burton et al. [9], Caramana et al. [10], Barlow [11], Love and Scovazzi [12], Kenamond et al. [13], and Llor et al. [14]. However, the algorithm complexity is important in the remap phase using staggered schemes in the context of ALE (Arbitrary Lagrangian Eulerian) or Lagrange-Remap schemes, where the velocity or momentum remap requires a special treatment and an additional correction to conserve total energy.

*Corresponding author
Email address: jean-philippe.braeunig@cea.fr (J.-P. Braeunig)
[1]For a historical overview see reminiscences about difference schemes in [3] and [4].

GLACE [15], published by Després and Mazeran in 2005, is the first collocated Lagrangian scheme which is also robust, followed by EUCCLHYD [1] in 2007. Both schemes are an inspiration to several other Lagrangian schemes such as Barlow and Roe (2010, [16]) and CCH (cell-centered hydrodynamics) developed by Burton et al. (2013, [17]), and to enhancements, for instance unstructured grids, axial symmetry, multi-dimensionality, second order, and Arbitrary Lagrangian-Eulerian (ALE) description, that are worth being mentioned (GLACE: [18, 19, 20]; EUCCLHYD: [21, 22, 23, 24, 25, 26]).

In these schemes acoustic Riemann solvers are used, which leads to an intrinsic entropy production. Recently, different approaches have been suggested in order to reduce this entropy. We cite the work of Cheng et al. [27], Liu et al. [28], and Boscheri et al. [29], that were able to reduce the global error of entropy with higher order schemes. Burton et al. [30] improved the second order CCH scheme with a higher order extension of the CGR (Corner Gradient Reconstruction) scheme and obtained an efficient reduction of the entropy production. With this method, viscous terms, which are calculated by acoustic Riemann solvers, are minimized.

In the context of our study we work on an Eulerian scheme of Lagrange-Remap type, whereas the Lagrangian phase uses the EUCCLHYD scheme and the remap phase (Chaudet and Braeunig [31]) uses alternate directions (AD) with interface reconstruction of PLIC (Piecewise Linear Interface Calculation) type. Our goal is to reduce the intrinsic entropy production, which can be observed in several schemes for hydrodynamics as mentioned above, by a correction on the face-fluxes. We work on a second order scheme and have in mind that higher order schemes could profit from this correction as well. We chose the EUCCLHYD scheme for the Lagrangian phase, because of its good properties: conservation of mass, momentum and total energy, respecting the GCL (Geometric Conservation Law), good robustness of the pure Lagrangian scheme mesh evolution, numerical pressure diffusion, numerical velocity diffusion and positive entropy production. In particular the EUCCHLYD scheme captures shock waves properly. However, the entropy production in isentropic flows is not negligible, particularly in the case of expansion waves, where it should be null. Braeunig has recently published two attempts to improve the EUCCHLYD method for isentropic flows: in the first one [32] he uses the total energy equation in compression and switches, depending on the satisfaction of a proposed conservation criterion, to internal energy equation in the case of expansion such that entropy production is nullified. This approach was not satisfactory as it cannot capture strong shock waves properly in all cases, since strict conservation is not ensured. With the second one [2], Braeunig suggests a correction strategy called Enhanced Entropy Behavior (EEB). He has added fluxes to the original scheme designed to annulate a part of the entropy production error, in a conservative way. If good properties of the original scheme are maintained with this correction, the dissipation reduction is not sufficient. In our framework, we use some ideas from this second publication. Particularly, we are interested in the definition of the partial entropy production, which is represented by the terms $q_{f,i}$ that quantify *entropy production in cell i due to the flux through face f*. With the help of these terms we are actually able to define an isentropic face-flux, which we apply in the case of expansion waves, i.e. when $\nabla.u > 0$ at f.

This report is structured in five sections: after the introduction, there is a theoretical section, in which the governing equations and numerical approaches are presented. Chapter 3 represents the main section, where we explain the new approach we call the *isentropic flux*, and how we apply it as a correction for the EUCCLHYD scheme in the case of expansion waves. We finish this report with some numerical results in chapter 4, followed by a conclusion.

2. Theoretical background

This section is a theoretical introduction to hydrodynamics in the context of our study, which deals with the *Lagrangian form* of the Euler equations. In the first paragraph, we state the *conservative form* of the Euler equations. Then, we introduce the *Lagrangian*, and *Eulerian* formalisms, discuss the discretization of the Euler system and derive the geometric conservation law (GCL). Afterwards, we apply the Godunov scheme on the obtained system, and describe the main steps of the EUCCLHYD algorithm. Furthermore, we introduce the *acoustic Godunov flux*, which is of main interest in this study. Finally, we conclude with an introduction to the *discretized entropy equation*, which is fundamental to our study of numerical dissipation.

2.1. Euler equations in conservative form

We introduce the Euler equations. It is a system of first order partial differential equations which describes the fluid motion of inviscid compressible fluids (liquid and gaseous):

$$\begin{cases} \partial_t \rho + \nabla.(\rho \vec{u}) = 0, \\ \partial_t (\rho \vec{u}) + \nabla.(\rho \vec{u} \otimes \vec{u}) + \nabla p = 0, \\ \partial_t (\rho E) + \nabla.(\rho E \vec{u}) + \nabla.(p \vec{u}) = 0, \end{cases} \tag{1}$$

where $\vec{u}$ denotes the velocity, ρ the density, E the total energy, which are functions of (x, t) and the pressure p is obtained through an Equation of State of variables (ρ, e), where e is the internal energy. Recall that the total energy is the sum of the internal energy and the kinetic energy: $E = e + \frac{\vec{u}^2}{2}$.

Adiabatic and inviscid flow is governed by these equations otherwise called continuity equation, momentum equation and energy equation.

2.2. Some manipulations on the Euler equations

First, we operate some manipulations on the Euler system by using the Reynolds transport formula. Second, we discretize the system. These equations are fundamental for the EUCCLHYD scheme, on which we operate in this work.

2.2.1. Applying the Reynolds transport formula

We directly apply the Reynolds transport formula on system (1) and use the *divergence theorem* and it yields:

$$\begin{cases} d_t \int_{\omega(t)} \rho \, d\omega = 0, \\ d_t \int_{\omega(t)} \rho u \, d\omega + \int_{\partial\omega(t)} p \, n \, ds = 0, \\ d_t \int_{\omega(t)} \rho E \, d\omega + \int_{\partial\omega(t)} ((pu) \cdot n) \, ds = 0, \end{cases} \tag{2}$$

where $\vec{n} = n$ defines the outward-pointing normal vector with respect to the control volume $\omega(t)$.

2.2.2. Discretization

We start from system (2) and evaluate the integrals on cell $\omega_i = \omega_i(t)$. The variables ρ, E, u and p on ω_i will be approximated by cell averaged values, thus homogeneous in cell. Let us introduce the discretized average variables $\overline{\rho_i}$, $\overline{E_i}$, $\overline{u_i}$ and $\overline{p_i}$, and define them for a discrete quantity a_i as follows:

$$\mathrm{Vol}_i \, \overline{a_i} = \int_{\omega_i} a_i \, d\omega. \tag{3}$$

Bringing together the derived formulas leads to the following *discretized system*, otherwise called *convective form*:

$$\begin{cases} d_t m_i & = 0, \\ \overline{\rho_i} d_t \overline{u_i} + \overline{\nabla_x p_i} & = 0, \\ \overline{\rho_i} d_t \overline{E_i} + \overline{\nabla_x.(p_i u_i)} & = 0, \end{cases} \tag{4}$$

with cell mass $m_i = \rho_i Vol_i$ and averaged gradient terms $\overline{\nabla_x p_i}$ and $\overline{\nabla_x.(p_i u_i)}$, which are flux terms defined through the numerical scheme.

2.3. Geometric conservation law (GCL)

Let us derive the volume conservation law, usually known under the name *geometric conservation law (GCL)* by using the Reynolds transport formula, which leads to the GCL:

$$d_t \int_{\omega(t)} d\omega - \int_{\omega(t)} \nabla_x.u \; d\omega = 0. \tag{5}$$

In order to discretize equation (5) we consider the averaged constant value of $\overline{\nabla_x.u_i}$ on cell i:

$$d_t \int_{\omega_i} d\omega - \int_{\omega_i} \nabla_x.u_i \; d\omega = d_t \mathrm{Vol}_i - \overline{\nabla_x.u_i} \; \mathrm{Vol}_i = 0. \tag{6}$$

Which leads to the following formula considering $d_t m_i = d_t(\overline{\rho_i} Vol_i) = 0$:

$$\boxed{\overline{\rho_i} d_t \frac{1}{\overline{\rho_i}} - \overline{\nabla_x.u_i} = 0} \tag{7}$$

In the litterature, the first equation of the discrete Euler system, i.e. the discrete continuity equation $d_t m_i = 0$, is often replaced by the GCL. These equations should be satisfied by the scheme at the discrete level. This explanation[2] was necessary to prevent confusion whenever we establish the Euler system in this equivalent formulation.

2.4. Godunov scheme applied to the Euler system

The discretized Euler system with $\mathcal{N}$ cells is written as:

$$\begin{cases} \overline{\rho_i} d_t(\frac{1}{\overline{\rho_i}}) - \overline{\nabla_x.u_i} = 0, \\ \\ \overline{\rho_i} d_t \overline{u_i} + \overline{\nabla_x p_i} = 0, & \forall i = 1, \ldots, \mathcal{N}, \\ \\ \overline{\rho_i} d_t \overline{E_i} + \overline{\nabla_x.(p_i u_i)} = 0. \end{cases} \tag{8}$$

In this notation the variable u is expressed as a non-specified multidimensional variable. Let us rewrite these equations in a compact form:

$$\overline{\rho_i} d_t \overline{W_i} + \overline{\nabla_x.\Phi_i} = 0, \qquad \text{with } \overline{W_i} = \begin{pmatrix} \overline{1/\rho_i}, \\ \overline{u_i} \\ \overline{E_i} \end{pmatrix}, \; \Phi_i = F(W_i) = \begin{pmatrix} -u^* \\ p^* \\ (pu)^* \end{pmatrix}. \tag{9}$$

Where $*$ indicates that these variables are solutions defined by a *Riemann problem*[3]. In order to create the scheme we multiply (9) by $\mathrm{Vol}_i = |\omega_i|$, keeping in mind that we evaluate Lagrangian variables on cell averaged values on cell ω_i:

$$\overline{\rho_i} \; |\omega_i| \; d_t \overline{W_i} + \int_{\omega_i} \nabla_x.\phi_i \; d\omega = 0. \tag{10}$$

Let us use Green's formula and now omit the *bar-notation* for the sake of a simple notation. Equation (10) writes:

$$d_t W_i + \frac{1}{\rho_i \; |\omega_i|} \sum_f A_f \; \Phi_{f,i} \; n_{f,i} = 0, \tag{11}$$

where f is a face of ω_i with area A_f, outward-pointing normal $n_{f,i}$ and *flux* vector $\Phi_{f,i}$.

Let us specify the 1D and 2D formulations of this Lagrangian scheme.

1D centered finite volume scheme

[2] More information about the GCL can be found in [24] or [33].

[3] [34] presents a main reference on this subject.

In the 1D case, the nodes coincide with the faces and are usually denoted by $x_{i-\frac{1}{2}}$ and $x_{i+\frac{1}{2}}$ for cell $\omega_i =]x_{i-\frac{1}{2}}, x_{i+\frac{1}{2}}[$. Let us numerate the two faces on cell ω_i and identify the index of the left face $i-\frac{1}{2}$ and analogously for the right face $i+\frac{1}{2}$. We then write $n_{i-\frac{1}{2}} = -1$ and $n_{i+\frac{1}{2}} = 1$ for a corresponding outward normal.

$$\frac{1/\rho_i^{n+1} - 1/\rho_i^n}{\Delta t} + \frac{1}{\rho_i^n \Delta x_i^n}(-u_{i+\frac{1}{2}}^n + u_{i-\frac{1}{2}}^n) = 0, \tag{12}$$

$$\frac{u_i^{n+1} - u_i^n}{\Delta t} + \frac{1}{\rho_i^n \Delta x_i^n}(p_{i+\frac{1}{2}}^n - p_{i-\frac{1}{2}}^n) = 0, \tag{13}$$

$$\frac{E_i^{n+1} - E_i^n}{\Delta t} + \frac{1}{\rho_i^n \Delta x_i^n}((pu)_{i+\frac{1}{2}}^n - (pu)_{i-\frac{1}{2}}^n) = 0, \tag{14}$$

where $\Delta t = t^{n+1} - t^n$ is the time step of the $(n+1)$th iteration and $\Delta x_i^n = \left|[x_{i-\frac{1}{2}}^n, x_{i+\frac{1}{2}}^n]\right| = x_{i+\frac{1}{2}}^n - x_{i-\frac{1}{2}}^n$ the length of cell ω_i^n in 1D.

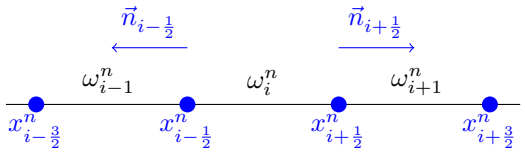

Figure 1: Discretization in 1D: The cells ω_i are the segments between the two nodes $x_{i+\frac{1}{2}}$ and $x_{i-\frac{1}{2}}$, where $i \in \{1, \ldots, \mathcal{N}\}$ and $\vec{n}_{i+\frac{1}{2}}, \vec{n}_{i-\frac{1}{2}}$ are the outward normals of cell ω_i. Remark that, whenever using a *Lagrangian* approach, the cells size may vary in each time iteration step.

2D centered finite volume scheme

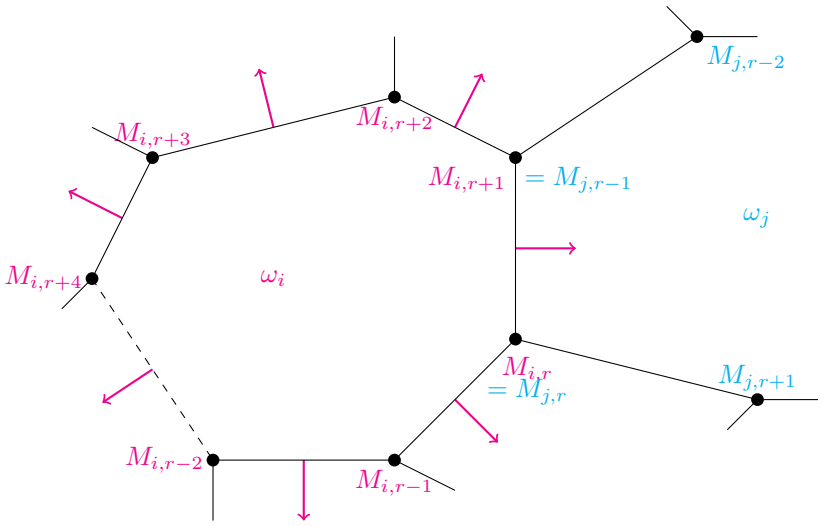

Figure 2: Space discretization in 2D: Grid with polygonal cells. The nodes of each cell are numbered in geometrical direction.

The 2D scheme is expressed as follows:

$$\frac{1/\rho_i^{n+1} - 1/\rho_i^n}{\Delta t} - \frac{1}{m_i}\sum_f A_f(u_f)n_{f,i} = 0, \tag{15}$$

$$\frac{u_i^{n+1} - u_i^n}{\Delta t} + \frac{1}{m_i}\sum_f A_f(p_{f,i})n_{f,i} = 0, \tag{16}$$

$$\frac{E_i^{n+1} - E_i^n}{\Delta t} + \frac{1}{m_i}\sum_f A_f((pu)_{f,i})n_{f,i} = 0, \tag{17}$$

$\forall i = 1, \ldots, \mathcal{N}$, where A_f is the area of face f (which corresponds to its length in 2D) and $n_{f,i} = \begin{pmatrix} n_x \\ n_y \end{pmatrix}_{f,i}$ its outward-pointing normal with respect to cell ω_i. The space discretization is expressed in terms of m_i, where $m_i = \rho_i|\omega_i|$. The face fluxes are noted with subscript (f, i) in order to refer to face f of cell ω_i. This is important to discuss in the context of the EUCCLHYD scheme, as it calculates two different values for the flux terms $p_{f,i}$ and $(pu)_{f,i}$, one for each side of the face, i.e. one for each cell. The velocity flux term on the other hand has the same value on each side of the face in the EUCCLHYD scheme, in which case we can leave out the index i and write u_f.
Figure 2 shows an unstructured grid, on which the formulation of the scheme presented in our main reference [1] is valid. The flux modification that will be described hereafter is designed to be possibly used to this type of mesh as well.

2.5. The EUCCLHYD solver: description of the algorithm

The EUCCLHYD (Explicit Unstructured Cell-Centered Lagrangian HYDrodynamics, [1]) scheme is constructed in 2D, and can be adapted in 1D and 3D. The scheme is collocated, which means that the cell variables are located at the cell center. Its main properties come from the *nodal solver* built by considering conservations and positive entropy production, and is such that in 1D it corresponds to the *Godunov acoustic Riemann solver*[4]. In the first step, the *nodal solver* computes the so-called *node velocities* and the *half edge pressures*, whereas the second step uses these quantities to obtain the face fluxes and in the third step the *physical variables* are updated. Let us introduce the discrete variables at the nodes and faces and specify the main steps of the scheme as follows:

1. Each node admits one *node velocity* u_r and twice as much *pressures at the half edges* than there are cells around the node. In order to simplify the notations used in the main reference of EUCCLHYD [1], we use a triple index (f, i, r) corresponding to face f, cell i and node r, which identifies the *half edge pressure* in a unique way, such that $p_{f,i,r}$ is the pressure on node r toward edge f on the side of cell i (see figure 1 below).

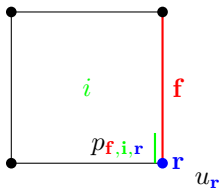

Figure 3: Illustration of *node velocity* u_r and *half edge pressure* $p_{f,i,r}$, with cell i, node r and face f.

2. The flux components on face f (on the side of cell i) are computed with the *node velocities* u_r, u_{r+1} and the *half edge pressures* $p_{f,i,r}$, $p_{f,i,r+1}$ as follows[5]:

[4] See paragraph 2.5.1
[5] Let us remark that the velocity flux term in the EUCCLHYD scheme is equal on both sides of a face f and denoted as u_f (instead of $u_{f,i}$).

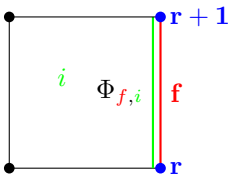

Figure 4: Flux $\Phi_{f,i} = (-u_f,\ p_{f,i},\ pu_{f,i})^t$ on face f on the side of cell i.

$$\left\{\begin{array}{rcl} u_f & = & \frac{1}{2}\left(u_r + u_{r+1}\right), \\ p_{f,i} & = & \frac{1}{2}\left(p_{f,i,r} + p_{f,i,r+1}\right), \\ (pu)_{f,i} & = & \frac{1}{2}\left(p_{f,i,r}u_r + p_{f,i,r+1}u_{r+1}\right). \end{array}\right. \tag{18}$$

3. The time step is governed by equations (15) to (17) and computes the specific volume $1/\rho$, the velocity $\vec{u}$, and the specific total energy E at time t^{n+1}. We reformulate these equations as follows[5]:

$$m_i\ d_t(1/\rho_i) - \sum_f A_f\ (u_f)\ n_{f,i} = 0, \tag{19}$$

$$m_i\ d_t u_i + \sum_f A_f\ (p_{f,i})\ n_{f,i} = 0, \tag{20}$$

$$m_i\ d_t E_i + \sum_f A_f\ ((pu)_{f,i})\ n_{f,i} = 0. \tag{21}$$

Where $d_t\mathcal{X}_i = \frac{\mathcal{X}_i^{n+1} - \mathcal{X}_i^n}{\Delta t}$ for any physical variable $\mathcal{X}_i$ on cell i with $\Delta t = t^{n+1} - t^n$, A_f is the area of face f, $n_{f,i}$ its outward normal unit vector and $\Phi_{f,i} = (-u_f,\ p_{f,i},\ pu_{f,i})^t$ the face flux calculated in the second step above.

2.5.1. Godunov's acoustic Riemann solver in 1D

Let us note the characteristics by $C^\lambda : \frac{dx}{dt} = \lambda$, which are defined by eigenvalues of the Euler equations system. Remember that the Riemann invariants of a PDE are constant on its characteristics. In order to construct the finite volume scheme based on a Riemann solver, we need to define how the information about the physical variables travels through the cells ω_i respecting the equations above. In other words we need to define the *discrete Riemann invariants*, taking into account the local flow variable on the characteristics $C^+ = C^{\lambda^+}$ and $C^- = C^{\lambda^-}$, where $\lambda^+ = c$ and $\lambda^- = -c$ are the characteristic velocities. These discrete equations will then allow us to calculate the flux $\Phi = \begin{pmatrix} -u^* \\ p^* \\ (pu)^* \end{pmatrix}$.

Let us explain this approach by means of Godunov's flux. To construct the *acoustic solver*, Godunov uses upwinded values of $(\rho\lambda^\pm)$ according to eigenvalues signs:

$$(\rho\lambda^+)_{i+\frac{1}{2}} = \rho_{i+\frac{1}{2}} c_{i+\frac{1}{2}} = \rho_i c_i, \tag{22}$$

$$(\rho\lambda^-)_{i+\frac{1}{2}} = \rho_{i+\frac{1}{2}}(-c_{i+\frac{1}{2}}) = -\rho_{i+1} c_{i+1}. \tag{23}$$

This choice allows us to write a discretized expression of the Riemann *invariants*, i.e. gives sense to $d_t p + \rho\lambda d_t u = 0$. In order to simplify the writing let us define $z_i := \rho_i c_i = (\rho c)_i$.

$$p_{i+\frac{1}{2}} - p_i + z_i(u_{i+\frac{1}{2}} - u_i) = 0, \quad \text{for } C^+, \tag{24}$$

$$p_{i+1} - p_{i+\frac{1}{2}} - z_{i+1}(u_{i+1} - u_{i+\frac{1}{2}}) = 0, \quad \text{for } C^-. \tag{25}$$

Further calculations on equations (24) and (25) lead to the following expression of $u_{i+\frac{1}{2}}$ and $p_{i+\frac{1}{2}}$:

$$u_{i+\frac{1}{2}} = \frac{z_i u_i + z_{i+1} u_{i+1} - (p_{i+1} - p_i)}{z_i + z_{i+1}}, \tag{26}$$

$$p_{i+\frac{1}{2}} = \frac{z_{i+1} p_i + z_i p_{i+1} - z_i z_{i+1}(u_{i+1} - u_i)}{z_i + z_{i+1}}, \tag{27}$$

where $z_i = (\rho c)_i$ and $\Phi = \begin{pmatrix} -u_{i+\frac{1}{2}} \\ p_{i+\frac{1}{2}} \\ p_{i+\frac{1}{2}} u_{i+\frac{1}{2}} \end{pmatrix} = \begin{pmatrix} -u^* \\ p^* \\ (pu)^* \end{pmatrix}$ is the flux vector of the acoustic Godunov solver. These fluxes have to be calculated first in order to solve equations (9). Generally one speaks about an *intermediate* iteration step. Recall that (12) will be the scheme we iterate in time in 1D.

2.6. The laws of thermodynamics and what they have to do with numerical dissipation

The first law of thermodynamics expresses the principle of energy conservation in a thermodynamical process. In fluid dynamics it is known as the *Gibbs formula*, which is written as follows:

$$m\, T\, d_t s = m\, d_t e + Vol\; p\, \nabla_x . u = m\, d_t E - m\, u d_t u + m\, p\, d_t(1/\rho), \tag{28}$$

using $e = E - E_{\text{kin}} = E - \frac{u^2}{2}$ and noting that $d_t E_{\text{kin}} = u\, d_t u$. We discretize $m\, T d_t s$ analogue to system (19) and call what follows the *discretized entropy equation*:

$$m_i^n T_i^n \frac{s_i^{n+1} - s_i^n}{\Delta t} = \sum_f A_f(-((pu)_{f,i}) + u_i^n(p_{f,i}) + p_i^n(u_f))\; n_{f,i}. \tag{29}$$

Remember that the second law of thermodynamics states that entropy production should be positive $d_t s \geq 0$. Whenever this is true at the discrete level for (29), we call the scheme *entropic*. We observe that this equation contains a sum of the flux vector components $\Phi = (-u,\; p,\; pu)^t$. Now let us clarify that these terms obviously are responsible for the production of the entropy in the discretized scheme.

In [1], authors construct the so-called *Nodal solver* such that the flux terms guarantee the positivity of the right hand side of (29), with a sum of squared terms.

3. Correction of the EUCCLHYD scheme for isentropic flows

In the previous chapter we have introduced the EUCCLHYD scheme and its theoretical background. Nevertheless, this flux correction could be an inspiration to other numerical schemes as well. The EUCCLHYD scheme produces too much entropy in expansion waves, which is an isentropic case. In this framework we propose a correction to improve accuracy in flows with expansions. We use some of the ideas from EUCCLHYD's entropy analysis exhibited by Braeunig [2]. Our goal is to present a correction of the flux terms, that we apply to the EUCCLHYD scheme.

3.1. Calculation of the isentropic flux

We want to compute the face-flux components u_f, $p_{f,i}$ and $(pu)_{f,i}$ in order to get an *isentropic flux*.[6] To do this we analyze the *discretized entropy equation* and determine from it the equations we need to finalize our calculations. Let us recall equation (29). We define Q_i as the right-hand side of the *semi-discrete entropy equation* and call it the *entropy production* in cell i:

$$Q_i \;:= \sum_f -A_f((pu)_{f,i})n_{f,i} + u_i A_f(p_{f,i})n_{f,i} + p_i A_f(u_f)n_{f,i}. \tag{30}$$

As we have mentioned before in section 2.6 this represents the dissipative term of the scheme. We also call it *numerical dissipation* and express the *discretized numerical entropy inequality* by $Q_i \geq 0$. Our goal is to reduce this term Q_i in the isentropic case, as it clearly should be equal to zero for expansion waves.

Let us consider cell Ω_i with its faces f. Integration on a closed volume area ensures that $\sum_f A_f n_{f,i} = 0$, which allows us to add this sum multiplied by $-p_i u_i$ to (30):

$$Q_i \;= \sum_f A_f(-((pu)_{f,i}) + u_i(p_{f,i}) + p_i(u_f) - p_i u_i)\; n_{f,i}. \tag{31}$$

[6] As mentioned before, in the case of EUCCLHYD the velocity flux term has the same value on each side of a face f and can be written as u_f.

Braeunig [2] has chosen this way of writing Q_i, such that each element in the sum on the right hand side of (31) can be recast as a positive square in the context of an acoustic Godunov flux in $1D$, of which we know the following:

$$m_i T_i d_t s_i = \rho_i c_i [(u_{f_1} - u_i)^2 + (u_{f_2} - u_i)^2] \geq 0. \tag{32}$$

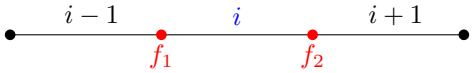

Figure 5: This figure illustrates the notation of the two faces f_1 and f_2 of cell i in $1D$.

We define the terms on the right hand side of (31), which Braeunig calls *entropy production in cell i due to the flux through face f*, as follows:

$$q_{f,i} := (-(((pu)_{f,i}) + u_i(p_{f,i}) + p_i(u_f) - p_i u_i)\, n_{f,i}, \tag{33}$$

Furthermore, we can confirm that $q_{f,i}$ in the specific case of an acoustic Godunov flux in $1D$, for which we have $(pu)_{f,i} = p_{f,i}u_f$, can be written as:

$$q_{f,i} = \rho_i c_i [(u_f - u_i)^2] \geq 0, \tag{34}$$

which coincides indeed with (32). This definition of $q_{f,i}$ given by (33) seems to be unique, since it is exclusively expressed with flux components at face f and values in cell i. **For all fluxes, except the acoustic Godunov flux, $q_{f,i}$ cannot stated to be positive** *a priori*. **It might be, but its value should be calculated and positivity studied with the considered flux components.**

We address here the improvement of expansion waves flows $\nabla_x u > 0$ only. Let us now consider two cells Ω_i and Ω_j, with their face $f = \Omega_i \cap \Omega_j$, in the expansion case. Locally at face f the flow is isentropic, i.e. the entropy production due to the flux through f should be null. Therefore, we set the following hypothesis on the terms $q_{f,i}$, $q_{f,j}$:[7]

$$\begin{cases} q_{f,i} = 0, \\ q_{f,j} = 0. \end{cases} \tag{35}$$

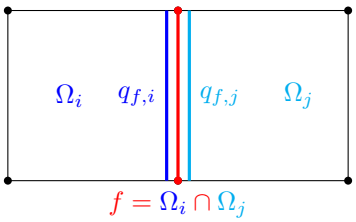

Figure 6: Illustration of the *entropy production* terms $q_{f,i}$ and $q_{f,j}$ on face $f := \Omega_i \cap \Omega_j$.

Let us note the new face flux, we call *isentropic flux*, with $\widehat{\Phi}_f = (-\widehat{u}_f,\ \widehat{p}_f,\ \widehat{pu}_f)^t$, where $\widehat{u}_f = u_f$, $\widehat{p}_f = \widehat{p}_{f,i} = \widehat{p}_{f,j}$ and $\widehat{pu}_f = \widehat{pu}_{f,i} = \widehat{pu}_{f,j}$. Hence, the hypotheses (35) give us the following system of two equations with the two unknowns $\widehat{p}_f$ and $\widehat{pu}_f$:

$$\begin{cases} A_f(-\widehat{pu}_f + u_i\widehat{p}_f + p_i\widehat{u}_f - p_i u_i)n_f = 0, \\ A_f(+\widehat{pu}_f - u_j\widehat{p}_f - p_j\widehat{u}_f + p_j u_j)n_f = 0. \end{cases} \tag{36}$$

[7] Recall that we introduced $q_{f,i}$ as the *entropy production in cell i due to the flux through face f* and analogously we say $q_{f,j}$ is the *entropy production in cell j due to the flux through face f*.

Recall that we define the normal by $n_f := n_{f,i} = -n_{f,j}$, where $n_{f,i}$ is the outward normal unit vector of cell i and $n_{f,j}$ of cell j (on face f). These two equations give us two constraints we need to calculate two of the three face-flux components $(-\widehat{u}_f,\ \widehat{p}_f,\ \widehat{pu}_f)^t$. Experiments with the original EUCCLHYD scheme show that the *Lagrangian* mesh moves properly and in a robust way. In order to keep this robust mesh behavior we choose to calculate the velocity $\widehat{u}_f$ the same as original EUCCLHYD solver, thus $\widehat{p}_f$ and $\widehat{pu}_f$ can be calculated using constraints (36). Let us use $q_{f,i} + q_{f,j} = 0$ to calculate $\widehat{p}_f$ from system (36):

$$\Rightarrow\ \widehat{p}_f = \frac{(u_i - \widehat{u}_f)n_f}{(u_i - u_j)n_f} p_i + \frac{(\widehat{u}_f - u_j)n_f}{(u_i - u_j)n_f} p_j. \tag{37}$$

We observe that the face pressure $\widehat{p}_f$ is therefore calculated by a weighted mean between the pressures on each cell, with the weights $\xi_i := \frac{(u_i - \widehat{u}_f)n_f}{(u_i - u_j)n_f}$ and $\xi_j := \frac{(\widehat{u}_f - u_j)n_f}{(u_i - u_j)n_f}$. Indeed, a simple calculation gives $\xi_i + \xi_j = 1$. Note that $(u_i - u_j)n_f > 0$ in the case of expansion and positivity of ξ is not granted in general, but it is enforced by considering the expansion criterion $u_i n_f > \widehat{u}_f n_f > u_j n_f$ to use the isentropic flux at face f.

Finally, we can calculate the third flux term $\widehat{pu}_f$ by either one equation of system (36):

$$\Rightarrow\ \widehat{pu}_f = \xi_j p_j u_i + \xi_i p_i u_j. \tag{38}$$

Remark 1. *We have to mention that previous studies to compute isentropic flows exist [35, 36] and inspired our work. For instance [36] presents a Tadmor-like flux*[8] *used in 1D for pure Lagrangian isentropic flows, with an obvious similarity to our isentropic flux, see Table 1. Proper comparison between these two fluxes are not presented here, since 1D results are close on the double rarefaction wave benchmark in section 4 and we did not encounter oscillations that have been mentioned by authors of [36] on a expansion in vacuum benchmark. We did not try further comparison since 2D flows are the subject of this paper, were no oscillations have been encountered with our scheme. Notice that whatever the velocity $\widehat{u}_f$ is, we always have $\widehat{u}_f = \xi_i u_j + \xi_j u_i$ by definition of ξ_i and ξ_j. We recall that u_f is here computed as the original EUCCLHYD scheme, giving Table 1 formula.*

Isentropic flux $\widehat{\mathbf{\Phi}}_\mathbf{f} = (-\widehat{\mathbf{u}_\mathbf{f}},\ \widehat{\mathbf{p}_\mathbf{f}},\ \widehat{\mathbf{pu}_\mathbf{f}})^\mathbf{t}$	***Tadmor-like* flux** $\mathbf{\Phi}_\mathbf{f}^\mathbf{T} = (-\mathbf{u}_\mathbf{f}^\mathbf{T},\ \mathbf{p}_\mathbf{f}^\mathbf{T},\ \mathbf{pu}_\mathbf{f}^\mathbf{T})^\mathbf{t}$
$\begin{cases} \widehat{u}_f &= u_f\ \ (= \xi_i u_j + \xi_j u_i) \\ \widehat{p}_f &= \xi_i\, p_i + \xi_j\, p_j \\ \widehat{pu}_f &= \xi_j p_j u_i + \xi_i p_i u_j \end{cases}$	$\begin{cases} u_f^T &= \alpha_j u_i + \alpha_i u_j \\ p_f^T &= \alpha_j p_j + \alpha_i p_i \\ (pu)_f^T &= \alpha_j p_j u_i + \alpha_i p_i u_j \end{cases}$
$\xi_i := \frac{(u_i - \widehat{u}_f)n_f}{(u_i - u_j)n_f},\ \xi_j := \frac{(\widehat{u}_f - u_j)n_f}{(u_i - u_j)n_f}$ $\xi_i + \xi_j = 1$	$\alpha_j := \frac{z_i}{z_i + z_j},\ \alpha_i := \frac{z_j}{z_i + z_j},\ z = \rho c$ $\alpha_i + \alpha_j = 1$

Table 1: Comparison between the *isentropic flux* and a *Tadmor-like* flux (presented in [36]).

3.2. Occurrence of expansion waves and algorithm for flux hybridization EUCCLHYD/Isentropic flux

Let us recall that we adapt our flux terms with the *isentropic flux* in the case of expansion waves only. In hydrodynamics an expansion is defined mathematically by $d_t \mathrm{Vol}/\mathrm{Vol} = \nabla.u > 0$. Once a face in expansion has been identified, we do a switch in order to calculate the new *isentropic flux* components, and only adjust the flux terms $p_{f,i}$ and $(pu)_{f,i}$ as illustrated in the flux hybridization algorithm below.

[8] Reference on the Tadmor flux: [37].

Algorithm Flux hybridization

input EUCCLHYD flux u_f, $p_{f,i}$, $(pu)_{f,i}$;
Cell variables ($\rightarrow$ *local load*);
for all Cells i **do**
  Load cell i and its neighbors;
  for all Faces f (with neighbor j) **do**
    if $u_j n_f > u_f n_f > u_i n_f$ **then**
      $p_{f,i} = \xi_i p_i + \xi_j p_j$;
      $(pu)_{f,i} = \xi_j p_j u_i + \xi_i p_i u_j$;
    end if
  end for
end for

3.3. Conservation of the scheme

The global conservation of the EUCCLHYD scheme is guaranteed by the following formula:

$$\sum_i m_i d_t V_i + \sum_i \sum_f A_f \Phi_{f,i} n_f = 0, \tag{39}$$

where $V_i = (1/\rho_i,\ u_i,\ E_i)^t$ and $\Phi_{f,i} = (-u_f,\ p_{f,i},\ pu_{f,i})^t$ the flux vector.

The EUCCLHYD fluxes have different values at both sides of a mesh face, calculated through the nodal solver that ensures local node centered conservations or in other words on the dual mesh. The isentropic correction proposed in this paper consists in replacing those fluxes with one unique *isentropic flux* at a face. This operation may break in 2D/3D the local conservation, only ensured in the frame of the standard EUCCLHYD solver. Since in 1D the EUCCLHYD scheme reduces to the Godunov acoustic scheme with a common value of flux at both sides of a face, the flux value can be modified with no care about conservation that is ensured by construction in Finite Volume schemes. The idea here is to add a correction to the isentropic flux in 2D/3D, to recover conservations as in the original EUCCLHYD scheme, and small enough to keep isentropic flux properties.

Construction of a conservative flux $\widetilde{\mathbf{\Phi}}_{\mathbf{f,i}} = (-\widetilde{\mathbf{u}}_{\mathbf{f}},\ \widetilde{\mathbf{p}}_{\mathbf{f,i}},\ \widetilde{\mathbf{pu}}_{\mathbf{f,i}})^{\mathbf{t}}$:

Let $\widehat{\Phi}_f = (-\widehat{u}_f,\ \widehat{p}_{f,i},\ \widehat{pu}_{f,i})^t$ be the *isentropic flux*. We define a conservative flux which satisfies equation (39) as follows:

$$\widetilde{\Phi}_{f,i} = \begin{cases} \Phi_{f,i} - \frac{\Phi_{f,i}+\Phi_{f,j(i)}}{2} + \widehat{\Phi}_f, & \text{if there is expansion at face } f, \\ \Phi_{f,i}, & \text{else.} \end{cases} \tag{40}$$

where $j(i)$ means the neighbor of i cell the other side of interface f, and $\Phi_{f,i} - (\Phi_{f,i} + \Phi_{f,j(i)})/2$ is supposed to be a small correction away from discontinuities since the gap between fluxes at both sides of the same face are driven by mesh geometry and pressure or velocity jumps.

Verification:

Recall that $n_f := n_{f,i} = -n_{f,j}$ is the outward normal of face f. Furthermore, a face is defined as the intersection of two cells c_i and c_j, i.e. $f := f_{i,j} = c_i \cap c_j$. Let us rewrite this sum as a sum over the faces (sum with index f):

$$\begin{aligned} \sum_i \sum_f A_f \widetilde{\Phi}_{f,i} n_f \quad &= \sum_{f:\text{ no expansion}} A_f(\Phi_{f,i} n_{f,i} + \Phi_{f,j} n_{f,j}) \\ &+ \sum_{f:\text{ expansion}} A_f \left(\frac{\Phi_{f,i} - \Phi_{f,j}}{2} n_{f,i} + \frac{\Phi_{f,j} - \Phi_{f,i}}{2} n_{f,j} \right) + \sum_{f:\text{ expansion}} A_f (\widehat{\Phi}_f n_{f,i} + \widehat{\Phi}_f \underbrace{n_{f,j}}_{=-n_{f,i}}). \end{aligned}$$

Rearranging terms considering $n_{f,j} = -n_{f,i}$, we obtain the global conservation (39) since:

$$\sum_i \sum_f A_f \widetilde{\Phi}_{f,i} n_f = \sum_f A_f (\Phi_{f,i} n_{f,i} + \Phi_{f,j} n_{f,j}) = \sum_i \sum_f A_f \Phi_{f,i} n_f.$$

4. Numerical results

In this section we briefly introduce the three benchmarks called Double rarefaction wave (DRW), Sedov, and Stony Brook. Each of these benchmarks is chosen for a particular reason. With the Double rarefaction wave (DRW) we observe the reduction of entropy production in the case of pure expansion waves. Sedov treats the case of a blast wave, where conservation laws have to be respected to obtain the right shock position (Rankine-Hugoniot jump relations), for which we do not want to change the good behavior of the EUCCLHYD scheme. Whereas Stony Brook represents a more complex case with the occurrence of the Richtmyer-Meshkov instability, which grows in an almost isentropic flow. These benchmarks were also discussed in [2].

We present the results of the scheme with the flux correction called *isentropic flux* compared to the original EUCCLHYD scheme implemented in the SHY code. The employed Lagrangian EUCCLHYD scheme is second order in time thanks to a two steps Runge-Kutta (or Predictor-Corrector) scheme and second order in space thanks to a MUSCL like multidimensional linear reconstruction at nodes, that all details may be found in Braeunig et al [32, 2]. The remap phase uses alternate directional splitting and is second order in space by classical linear MUSCL reconstruction. The total energy remap flux uses modification presented in [32] to lower the internal energy loss when using high order conservative schemes. The chosen limiter for both phases is VanLeer. Multimaterial interface reconstruction is of VOF Youngs PLIC type [8] with homogeneous distribution of specific entropy between materials in mixed cells, as described in [32]. These features have shown good behavior in most cases with no tricks needed and robust for CFL time constraint coefficients up to 0.6 in 1D and 0.4 in 2D.
We implemented both the conservative version of the isentropic flux described in chapter 3.3 and the initial version stated in table 1. However, in 1D there is no difference to observe between the isentropic flux and its conservative version, as they are the same flux in 1D. We use ParaView to display the results. Mostly, we are interested in the results obtained by the Lagrange EUCCLHYD-Remap scheme. However, we will show pure Lagrangian results as well for the double rarefaction wave test case. The analytic solutions are drawn in black, the results obtained with original EUCCLHYD are represented with dashed lines, whereas its correction with the new flux shows solid lines.

4.1. Double rarefaction wave (DRW) Lagrange-Remap

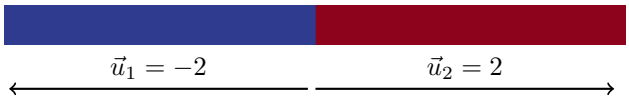

Figure 7: 1D test case of two rarefaction waves moving away from the center.

	Material 1	Material 2	unit
Density ρ	1.	1.	kg/m^3
Pressure p	0.4	0.4	Pa
Velocity u	-2.	2.	m/s
Adiabatic index γ	1.4	1.4	

Table 2: Initial state of the DRW benchmark. Remark that the pressure is defined by the equation of state (EOS) $p = p(\rho, e) = \rho(\gamma - 1)e$.

In this benchmark, the 1D domain is splitted in two symmetric regions. In the initial state the two fluids have the same constant density and pressure, whereas their velocity goes in opposite directions as indicated in figure

7 above. The simulation shows two expansion waves in outwards direction away from the center and it ends at $t = 0.16$. We chose this benchmark to observe the effect of our correction with the new *isentropic flux* in this isentropic flow. We investigated the cases of 201 and 2001 cells, odd numbers of cells with $u = 0$ in the central cell imposed by domain symmetry. The case with even number of cells causes a spurious entropy behavior provoked by a very stiff initialization of velocity and a degenerated flux at the face at the center of the domain due to symmetry. So we have decided to avoid this situation that is not relevant for real geometry simulations.Boundary conditions should be Neumann as described for EUCCLHYD in [1], to keep outward velocity and unchanged states before the expansion arrives to the domain borders [1,2]. Actually, a fictional [0,3] domain is used to keep real domain [1,2] away from borders influence. Figures 8 and 9 show the results obtained at $t = 0.16$ for the internal energy and entropy. We observe that we were able to reduce the entropy with the new *isentropic flux* correction compared to EUCCLHYD's original version. Furthermore, the entropy stays positive as it should. Results obtained with isentropic flux conservation modification or without are identical, since those fluxes are the same in 1D.

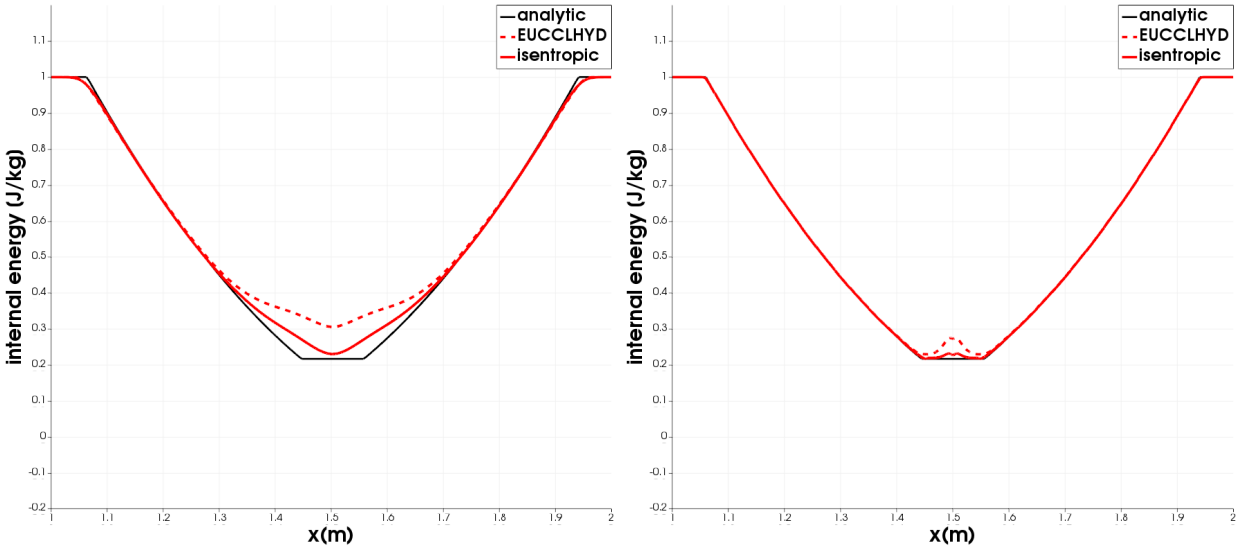

Figure 8: Eulerian Lagrange-Remap scheme, Internal energy. Mesh with 201 cells (left) and 2001 cells (right).

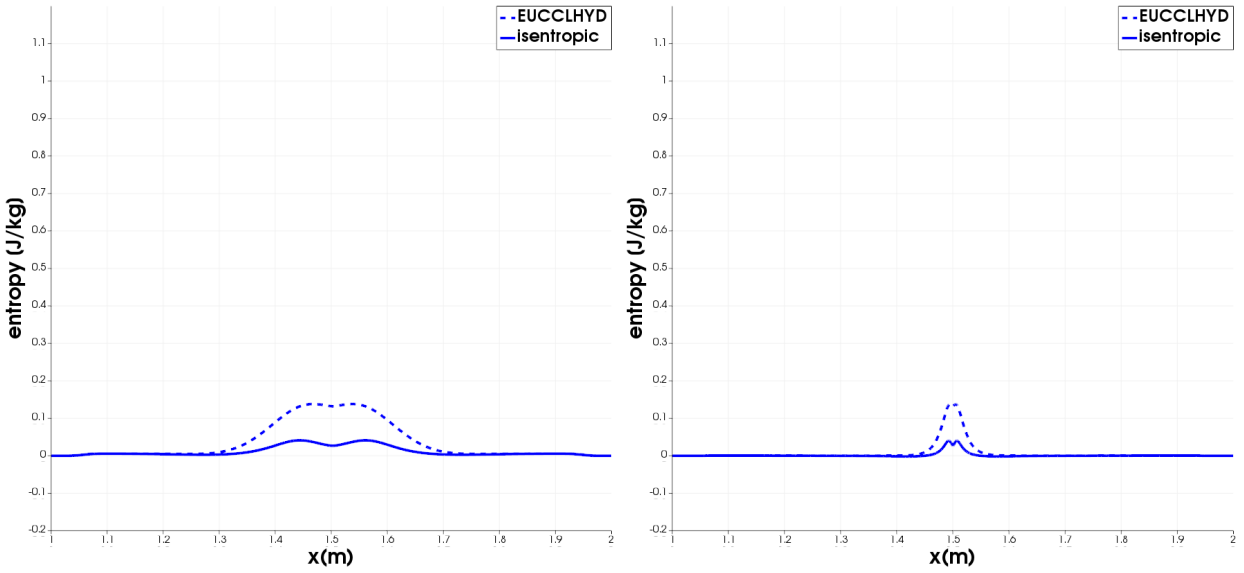

Figure 9: Eulerian Lagrange-Remap scheme, Entropy. Mesh with 201 cells (left) and 2001 cells (right).

4.2. Double rarefaction wave (DRW) in pure Lagrangian form

Let us investigate in this section the entropy reduction in the Lagrangian phase. We present the results of the internal energy and entropy, obtained with the pure Lagrangian scheme (i.e. without a remap after the Lagrangian phase), therefore letting the mesh move with the flow. We keep exactly the same set-up as stated in the previous section about DRW with the Eulerian scheme.

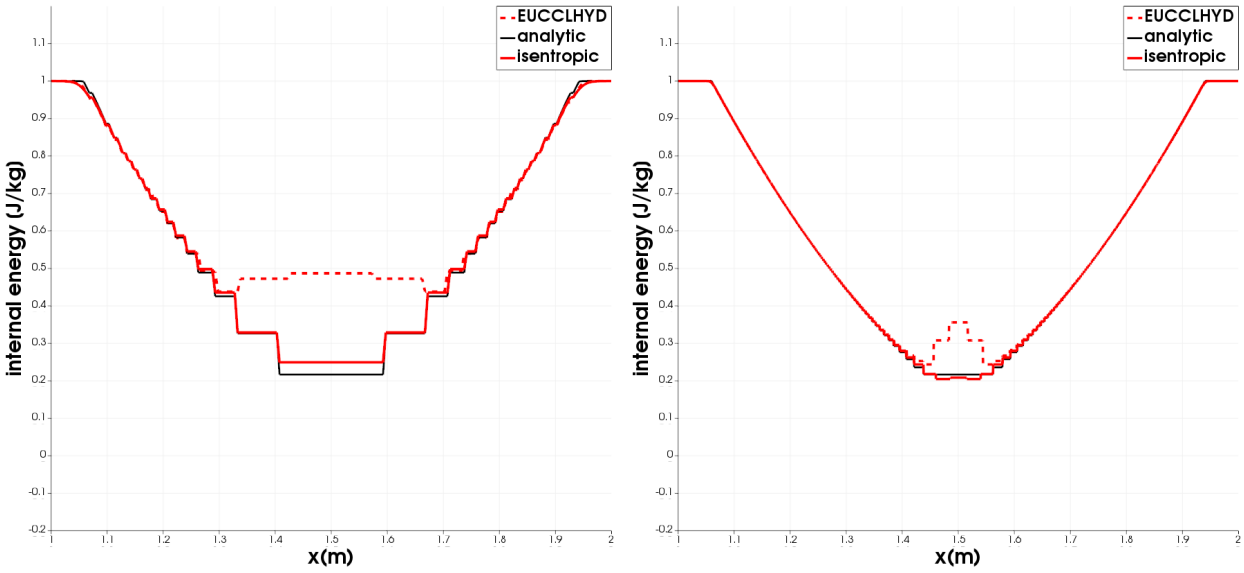

Figure 10: Pure Lagrangian scheme, Internal energy. Mesh which had initially 201 cells (left) and 2001 cells (right).

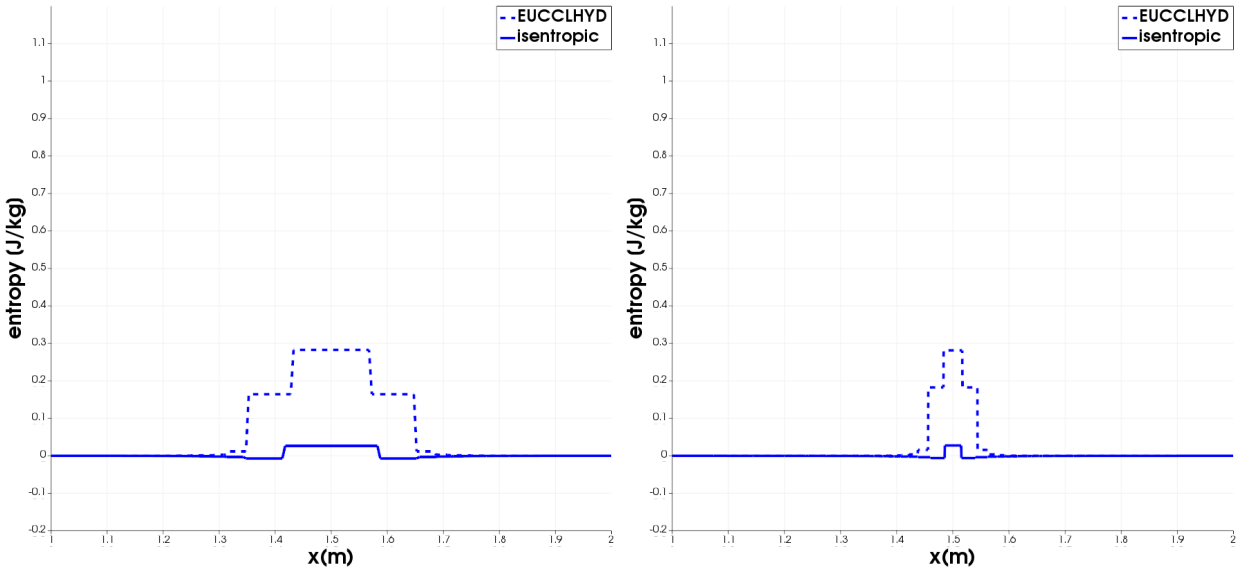

Figure 11: Pure Lagrangian scheme, Entropy. Mesh which had initially 201 cells (left) and 2001 cells (right).

In this Lagrangian simulation the mesh moves in direction of the fluid flow and consequently the cells in the center expand, whereas the cells on both ends disappear by crossing the domain boundaries. The plots generated with ParaView [38] automatically extend the values of the cell-parameters to the whole cell. Thus, the solution on a expanded mesh is drawn as a bar, which indicates the length of the cells. The results obtained in this pure Lagrangian simulation underline the reduction of the entropy production in the Lagrangian phase with our flux correction.

4.3. Sedov Lagrange-Remap

Sedov is a two dimensional benchmark on a 2D domain of size 1.1×1.1 meshed with 110×110 cells. Initially there is a high amount of energy deposited on one cell down left. As a consequence the cell explodes and a spherical blast wave propagates outwards. This set-up shows a quarter of the blast wave. We stop the iterations at $t = 1$, where the propagation has theoretically reached a radius of $x = 1$.

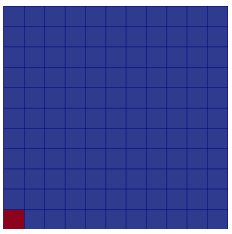

Figure 12: Initial state of the internal energy. Explosion in one cell down left.

	Material 1	Material 2	unit
Density ρ	1.	1.	kg/m^3
Velocity u	0.	0.	m/s
Internal energy e	2448.16	10^{-16}	J/kg
Adiabatic index γ	1.4	1.4	

Table 3: Initial state of the Sedov benchmark.

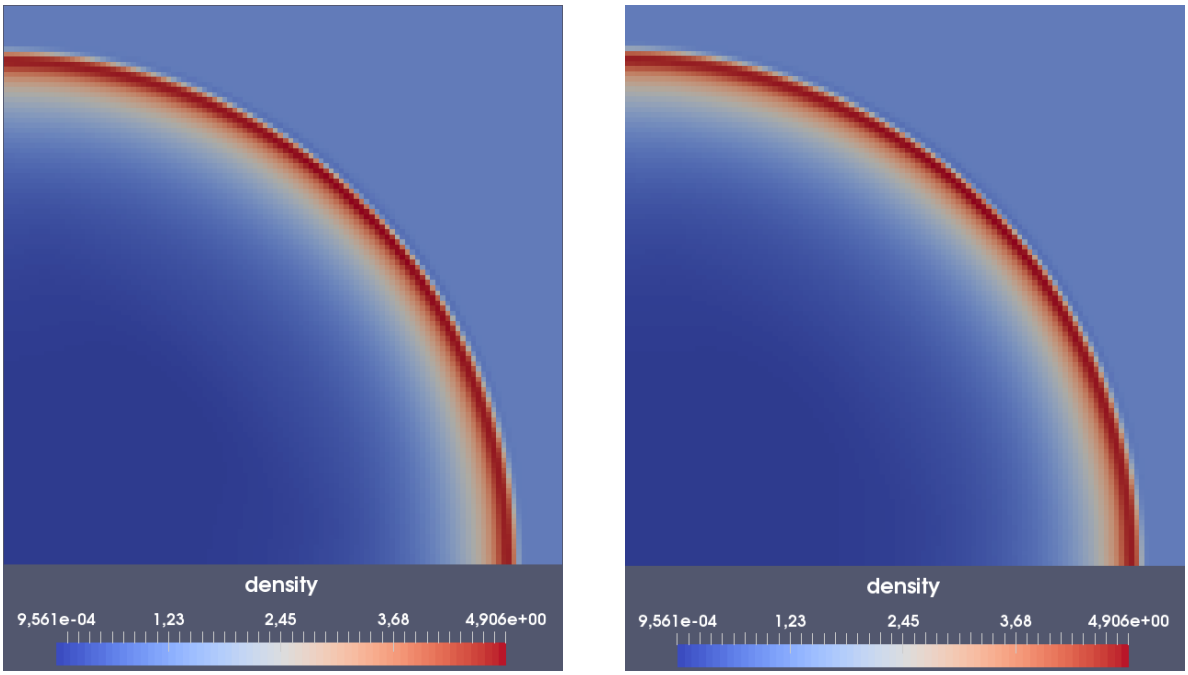

Figure 13: Eulerian Lagrange-Remap scheme, final state of the density with the EUCCLHYD scheme (left) and the conservative isentropic flux correction (right). The explosion has propagated.

We observe on figures 13 to 15 that the conservative version of the isentropic flux does not modify the solution of the original EUCCLHYD scheme. This is an important result, as it ensures that the shock waves capturing ability is not affected by the isentropic flux correction.
When using the non conservative isentropic flux, i.e. without using correction from paragraph 3.3, results are slightly modified in $x = y$ line cut compared to the original scheme, see figures 16 and 17. However, results are good in x and y directions, since this scheme is conservative in 1D and since the flow is quasi-1D in mesh principal directions.

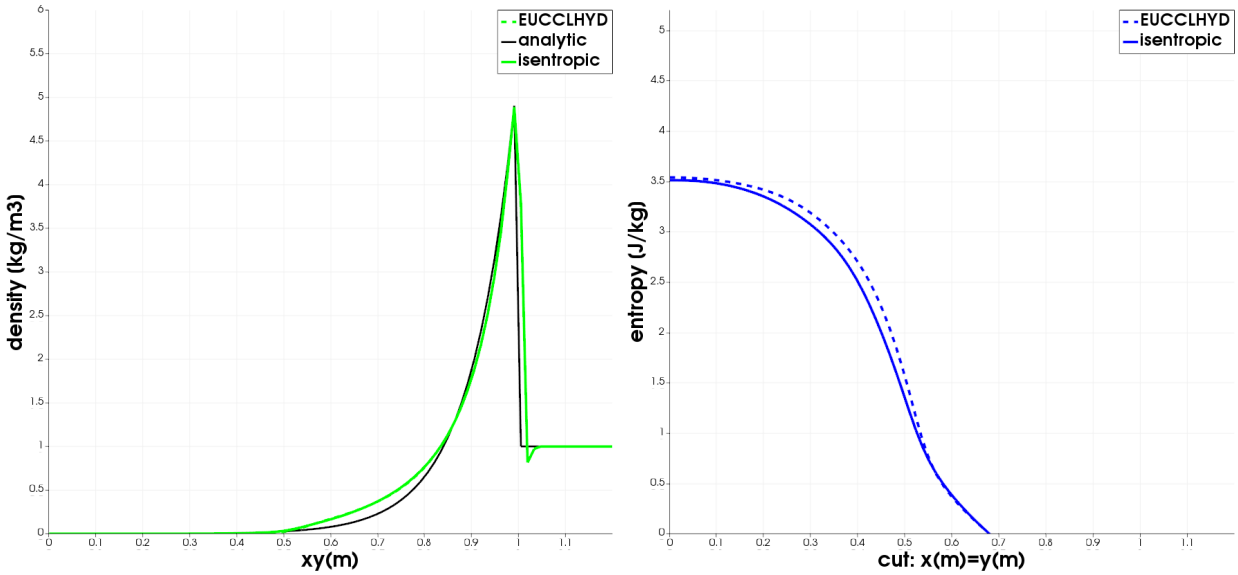

Figure 14: Eulerian Lagrange-Remap scheme, conservative flux correction: density (left), entropy (right). Diagonal cut (x=y): 110 cells.

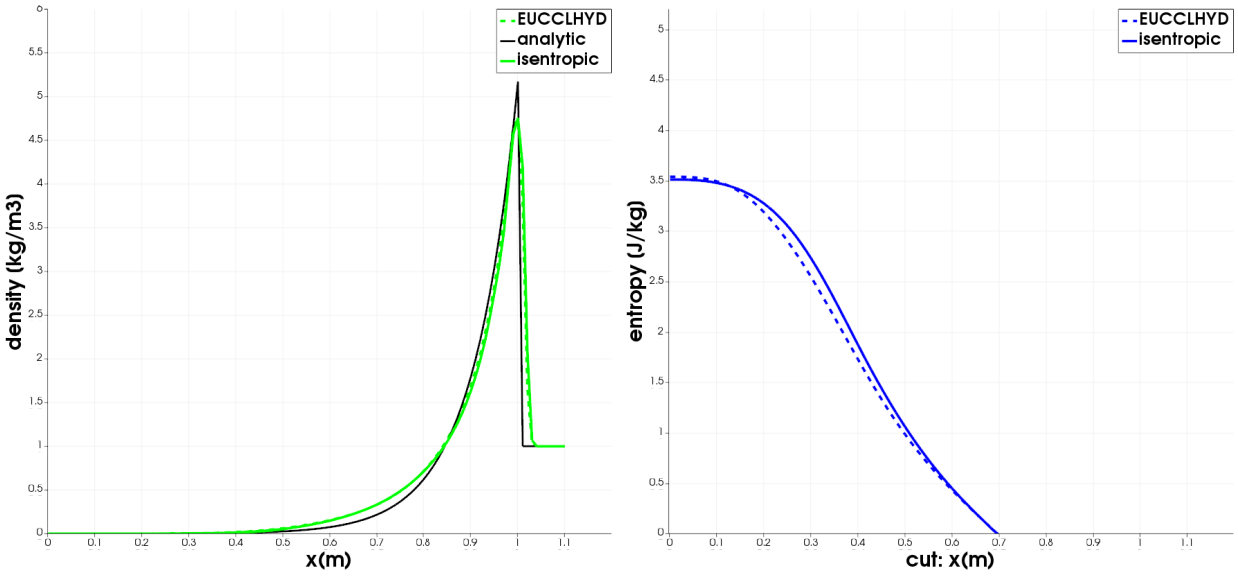

Figure 15: Eulerian Lagrange-Remap scheme, conservative flux correction: density (left), entropy (right). x-axis cut: 110 cells.

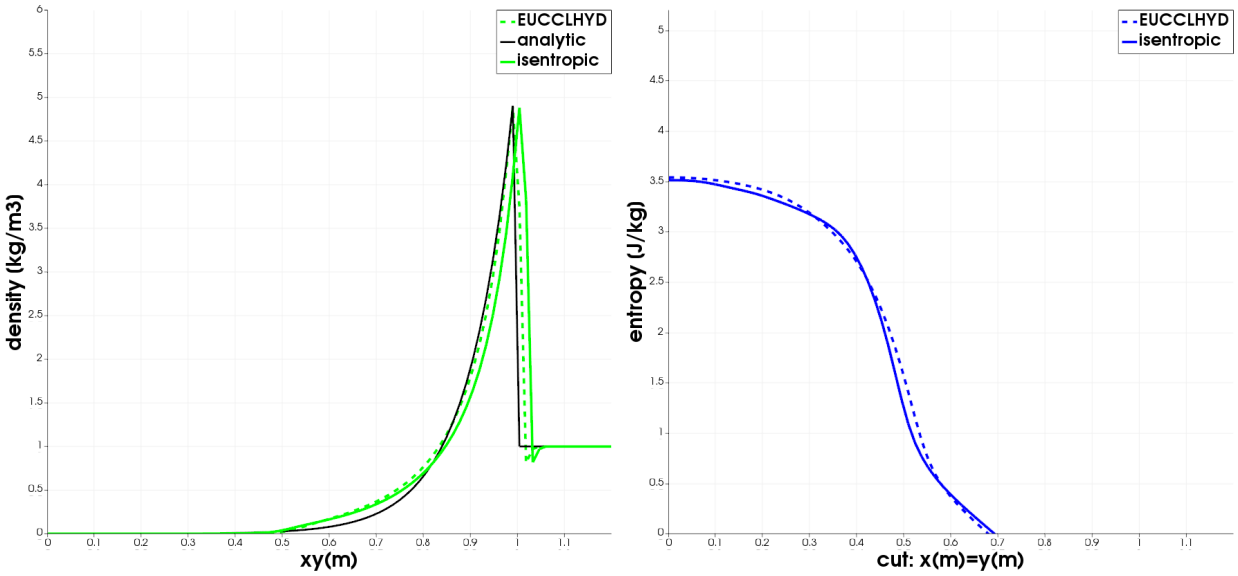

Figure 16: Eulerian Lagrange-Remap scheme, non conservative flux correction: density (left), entropy (right). Diagonal cut (x=y): 110 cells.

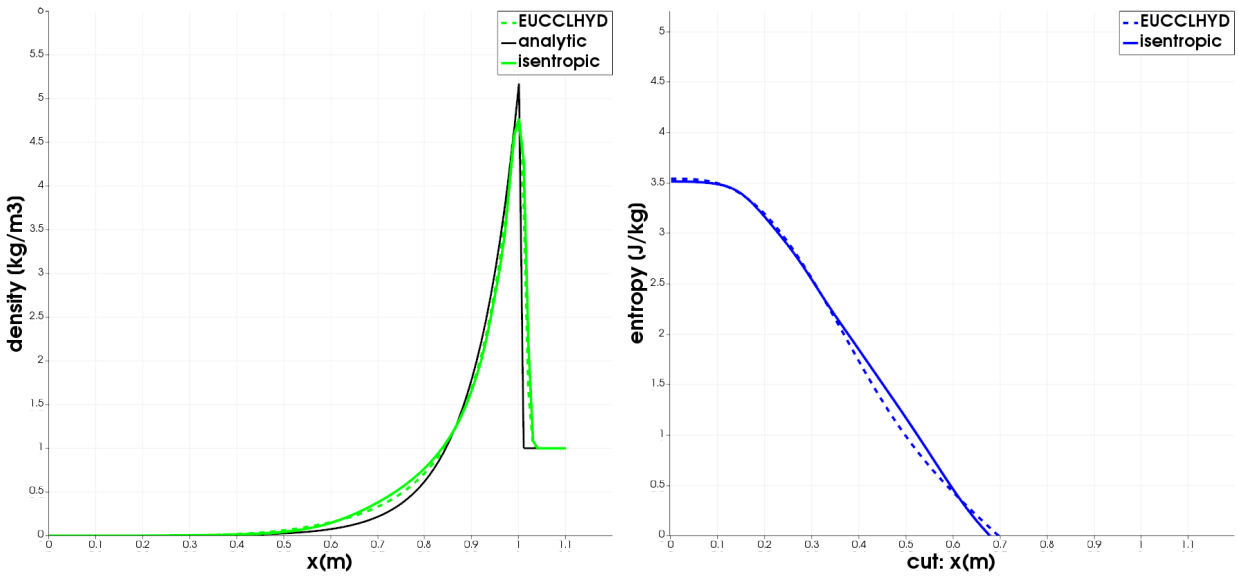

Figure 17: Eulerian Lagrange-Remap scheme, non conservative flux correction: density (left), entropy (right). x-axis cut: 110 cells.

4.4. Stony Brook Lagrange-Remap

Figure 18: Two materials initialized with a perturbed interface (sinusoidal).

In the Stony Brook benchmark we have two materials of different acoustic impedances (material 1 on the left and material 2 on the right) separated by a perturbed (sinusoidal) interface as shown in figure 18. The interface is captured in its motion by a PLIC-like method, described in [31]. There is a shock wave coming from the right-hand side through material 2 in direction of material 1. The shock front is initialized at $x = 33$, which indicates that the shock wave already passed through material 2 at the initial state. This is illustrated in figure 19. Boundary conditions should be Neumann as described for EUCCLHYD in [1] but when the shock or expansion waves hit the borders, they are reflected on it. It is necessary to use a long shock tube $[0,\ 80]$ with width $[0,\ 1.8]$, in which interface is centered at abscissa $x = 30$, see Figure 19, to prevent the interface from borders influence until end time. All figures about this test case are zooms on the interface, not representing the whole length of the domain.

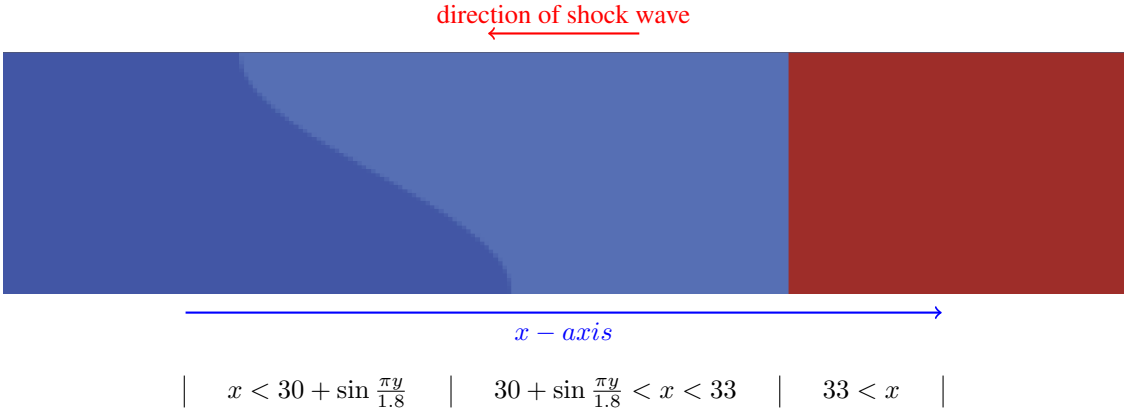

Figure 19: Initialization of the shock-front in material 2 at $x = 33$.

	Material 1	Material 2	Material 2	unit
Density ρ	$2.95\ 10^{-3}$	$1.87\ 10^{-3}$	$6.01\ 10^{-3}$	kg/m^3
Velocity u	$45.3\ 10^{3}$	$45.3\ 10^{3}$	$-5.55\ 10^{3}$	m/s
pressure p	$75.3\ 10^{5}$	$5.\ 10^{5}$	$5.\ 10^{5}$	Pa
Adiabatic index γ	1.666	1.666	1.666	

Table 4: Initial state of the Stony Brook benchmark.

Once the shock front has passed the interface, we observe the phenomena known as *Richtmyer-Meshkov instability* (RMI). Vorticity is deposited at the interface and a *mushroom* shape is developed in almost isentropic flow. The scheme uses a PLIC-like interface reconstruction algorithm[9].
Figures 20 to 22 show more roll up with the isentropic flux correction (top) than with conservative correction (middle). Figure 23 shows vorticity profiles $\nabla \times u \cdot e_z$, with same scale for all schemes. Figure 24 shows the maximum of vorticity versus time for each scheme, that gives a quantitative measure to compare them. Therefore, correction for conservation adds dissipation in the vortex compare to the isentropic flux. However, we observe an improvement compared to the solution of the original EUCCLHYD scheme. We conclude that as entropy production is reduced with this new flux, so more kinetic energy or vorticity is kept in the vortex, so more roll up of the mushroom.

[9] Braeunig and Chaudet [31]

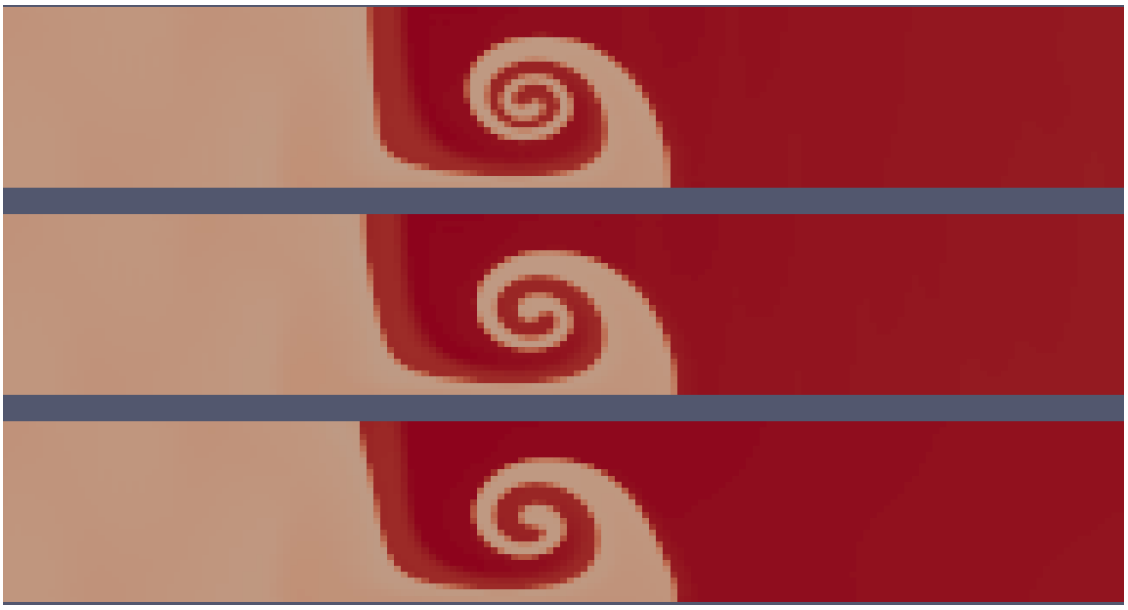

Figure 20: Eulerian Lagrange-Remap scheme, internal energy profiles Stony Brook benchmark at end time ($\approx$ 7 10^{-3}s, 1200 $\times$ 30 cells). Top: isentropic flux, middle: conservative isentropic flux, bottom: EUCCLHYD.

Figure 21: Eulerian Lagrange-Remap scheme, internal energy profiles Stony Brook benchmark at end time($\approx$ 5 10^{-3}s, 2400 $\times$ 60 cells). Top: isentropic flux, middle: conservative isentropic flux, bottom: EUCCLHYD.

Figure 22: Eulerian Lagrange-Remap scheme, internal energy profiles Stony Brook benchmark at end time($\approx$ 7 10^{-3}s, 2400 $\times$ 60 cells). Top: isentropic flux, middle: conservative isentropic flux, bottom: EUCCLHYD.

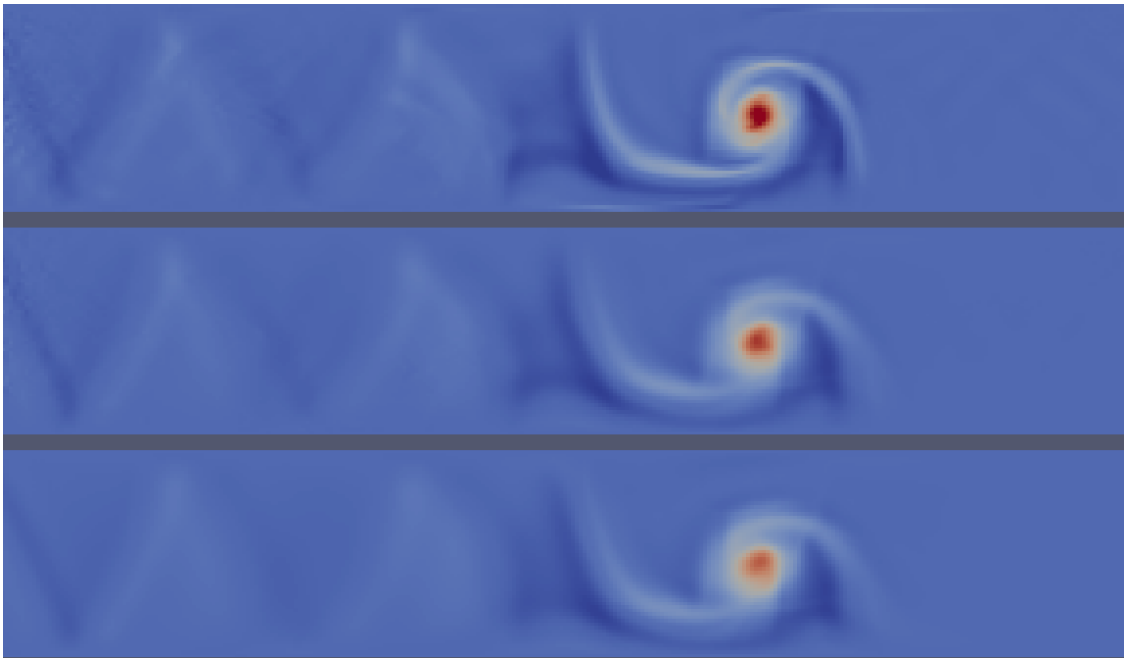

Figure 23: Eulerian Lagrange-Remap scheme, vorticity $\nabla \times u \cdot e_z$ profiles with same scale, Stony Brook benchmark at end time($\approx$ 7 10^{-3}s, 2400 $\times$ 60 cells). Top: isentropic flux, middle: conservative isentropic flux, bottom: EUCCLHYD.

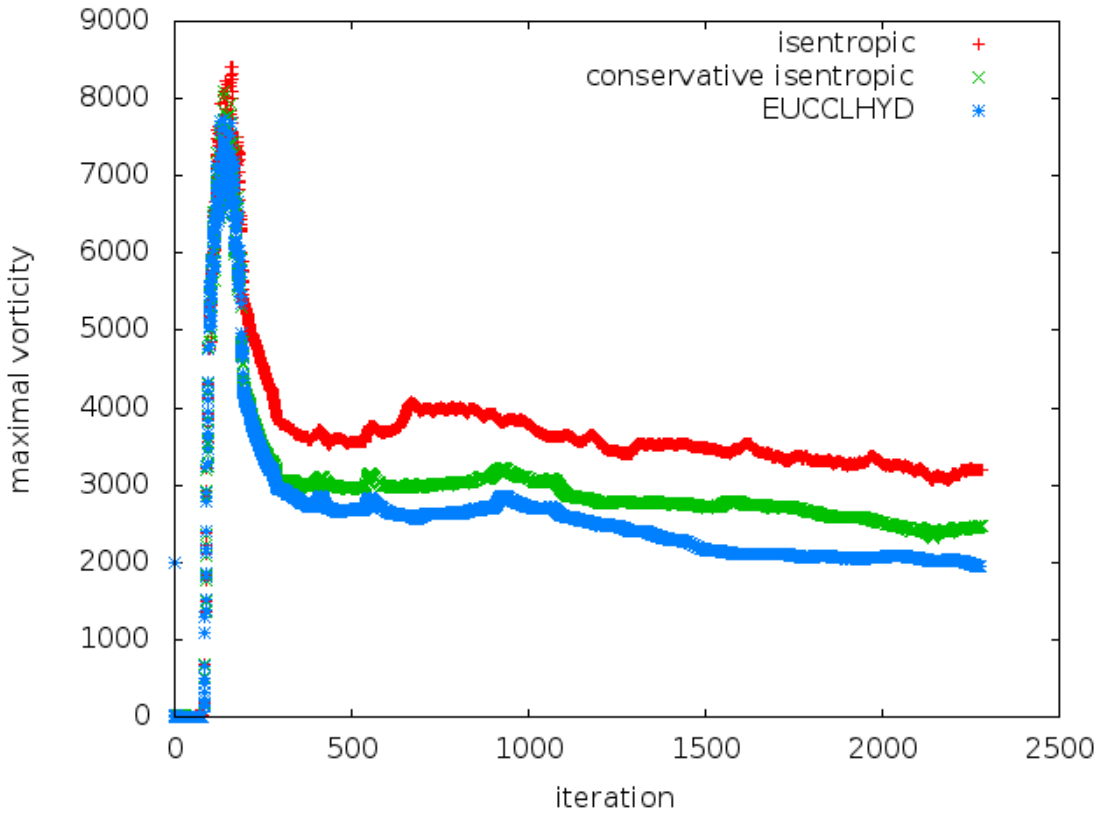

Figure 24: Eulerian Lagrange-Remap scheme, maximum of vorticity $\nabla \times u \cdot e_z$ for Stony Brook benchmark versus time, 2400×60 cells) for isentropic flux, conservative isentropic flux, EUCCLHYD.

5. Conclusion

We have applied the flux correction developed in this work on the EUCCLHYD-Remap scheme implemented in SHY, a research code dedicated to numerical scheme studies, where a PLIC-like interface capturing method is available. This gave us promising results, especially for the Double rarefaction wave (DRW) benchmark and Stony Brook, where the numerical entropy production in expansion waves, that should be null, has been reduced meaningfully. On the other hand, we showed with the Sedov test case that accuracy of EUCCLHYD is not altered in the case of strong shock waves, when using the conservative version of this isentropic flux. This last version of the scheme shows more numerical dissipation than the initial isentropic flux. This point will be investigated further, especially to integrate the isentropic flux form exhibited in this work directly as a modification of the nodal solver, in an intrinsic conservative way that would avoid a flux correction. Furthermore, SHY is yet implemented for structured rectangular meshes. The EUCCLHYD scheme and the correction proposed in this framework are also valid for unstructured grids, where two distinct nodes do not necessarily have the same number of adjacent faces. The proposed flux correction shows no obstacle in this context.

References

[1] P.-H. Maire, R. Abgrall, J. Breil, J. Ovadia, A cell-centered Lagrangian scheme for two-dimensional compressible flow problems, SIAM Journal on Scientific Computing 29 (4) (2007) 1781–1824.

[2] J.-P. Braeunig, Reducing the entropy production in a collocated Lagrange–Remap scheme, Journal of Computational Physics 314 (2016) 127–144.

[3] S. K. Godunov, Reminiscences about difference schemes, Journal of Computational Physics 153 (1) (1999) 6–25.
[4] B. van Leer, An introduction to the article "reminiscences about difference schemes" by sk godunov, Journal of Computational Physics 153 (1) (1999) 1–5.
[5] S. K. Godunov, A difference method for numerical calculation of discontinuous solutions of the equations of hydrodynamics, Matematicheskii Sbornik 89 (3) (1959) 271–306.
[6] J. Von Neumann, R. D. Richtmyer, A method for the numerical calculation of hydrodynamic shocks, Journal of applied physics 21 (3) (1950) 232–237.
[7] M. L. Wilkins, Calculation of elastic-plastic flow, Tech. rep., California Univ Livermore Radiation Lab (1963).
[8] D. Youngs, Time-dependent multi-material flow with large fluid distortion, Numerical Methods for Fluid Dynamics 1 (1982) 273–285.
[9] D. E. Burton, Exact conservation of energy and momentum in staggered-grid hydrodynamics with arbitrary connectivity, in: Advances in the Free-Lagrange Method Including Contributions on Adaptive Gridding and the Smooth Particle Hydrodynamics Method, Springer, 1991, pp. 7–19.
[10] E. Caramana, D. Burton, M. Shashkov, P. Whalen, The construction of compatible hydrodynamics algorithms utilizing conservation of total energy, Journal of Computational Physics 146 (1) (1998) 227–262.
[11] A. J. Barlow, A compatible finite element multi-material ALE hydrodynamics algorithm, International journal for numerical methods in fluids 56 (8) (2008) 953–964.
[12] E. Love, G. Scovazzi, On the angular momentum conservation and incremental objectivity properties of a predictor/multi-corrector method for lagrangian shock hydrodynamics, Computer Methods in Applied Mechanics and Engineering 198 (41) (2009) 3207–3213.
[13] M. Kenamond, M. Bement, M. Shashkov, Compatible, total energy conserving and symmetry preserving arbitrary Lagrangian–Eulerian hydrodynamics in 2D rz-cylindrical coordinates, Journal of Computational Physics 268 (2014) 154–185.
[14] A. Llor, A. Claisse, C. Fochesato, Energy preservation and entropy in lagrangian space-and time-staggered hydrodynamic schemes, Journal of Computational Physics 309 (2016) 324–349.
[15] B. Després, C. Mazeran, Lagrangian gas dynamics in two dimensions and Lagrangian systems, Archive for Rational Mechanics and Analysis 178 (3) (2005) 327–372.
[16] A. Barlow, P. Roe, A cell centred Lagrangian Godunov scheme for shock hydrodynamics, Computers & Fluids 46 (1) (2011) 133–136.
[17] D. Burton, T. Carney, N. Morgan, S. Sambasivan, M. Shashkov, A cell-centered Lagrangian Godunov-like method for solid dynamics, Computers & Fluids 83 (2013) 33–47.
[18] G. Carré, S. Del Pino, B. Després, E. Labourasse, A cell-centered Lagrangian hydrodynamics scheme on general unstructured meshes in arbitrary dimension, Journal of Computational Physics 228 (14) (2009) 5160–5183.
[19] B. Després, Weak consistency of the cell-centered Lagrangian GLACE scheme on general meshes in any dimension, Computer Methods in Applied Mechanics and Engineering 199 (41) (2010) 2669–2679.
[20] G. Kluth, B. Després, Discretization of hyperelasticity on unstructured mesh with a cell-centered Lagrangian scheme, Journal of Computational Physics 229 (24) (2010) 9092–9118.
[21] S. Galera, P.-H. Maire, J. Breil, A two-dimensional unstructured cell-centered multi-material ALE scheme using VOF interface reconstruction, Journal of Computational Physics 229 (16) (2010) 5755–5787.
[22] S. Galera, J. Breil, P.-H. Maire, A 2D unstructured multi-material Cell-Centered Arbitrary Lagrangian–Eulerian (CCALE) scheme using MOF interface reconstruction, Computers & Fluids 46 (1) (2011) 237–244.
[23] P.-H. Maire, A high-order cell-centered Lagrangian scheme for two-dimensional compressible fluid flows on unstructured meshes, Journal of Computational Physics 228 (7) (2009) 2391–2425.
[24] P.-H. Maire, A unified sub-cell force-based discretization for cell-centered Lagrangian hydrodynamics on polygonal grids, International Journal for Numerical Methods in Fluids 65 (11-12) (2011) 1281–1294.
[25] P.-H. Maire, J. Breil, A second-order cell-centered Lagrangian scheme for two-dimensional compressible flow problems, International journal for numerical methods in fluids 56 (8) (2008) 1417–1423.
[26] P.-H. Maire, B. Nkonga, Multi-scale Godunov-type method for cell-centered discrete Lagrangian hydrodynamics, Journal of Computational Physics 228 (3) (2009) 799–821.
[27] J. Cheng, C.-W. Shu, A high order ENO conservative Lagrangian type scheme for the compressible Euler equations, Journal of Computational Physics 227 (2) (2007) 1567–1596.
[28] W. Liu, J. Cheng, C.-W. Shu, High order conservative Lagrangian schemes with Lax–Wendroff type time discretization for the compressible Euler equations, Journal of Computational Physics 228 (23) (2009) 8872–8891.
[29] W. Boscheri, M. Dumbser, A direct Arbitrary–Lagrangian–Eulerian ADER–WENO finite volume scheme on unstructured tetrahedral meshes for conservative and non-conservative hyperbolic systems in 3D, Journal of Computational Physics 275 (2014) 484–523.
[30] D. E. Burton, N. R. Morgan, T. C. Carney, M. A. Kenamond, Reduction of dissipation in Lagrange cell-centered hydrodynamics (CCH) through corner gradient reconstruction (CGR), Journal of Computational Physics 299 (2015) 229–280.
[31] J.-P. Braeunig, B. Chaudet, Study of a collocated Lagrange–Remap scheme for multi-material flows adapted to HPC, International Journal for Numerical Methods in Fluids 83 (8) (2017) 664–678.
[32] J.-P. Braeunig, Study of a collocated Lagrange–Remap scheme for multi-material flows adapted to HPC, in: MULTIMAT conference, 2015, würzburg, Germany.
[33] P.-H. Maire, Contribution to the numerical modeling of inertial confinement fusion, Ph.D. thesis, Université Bordeaux I (2011).
[34] E. Godlewski, P. Raviart, Numerical Approximation of Hyperbolic Systems of Conservation Laws, no. no. 118 in Applied Mathematical Sciences, Springer, 1996.
URL https://books.google.fr/books?id=9BwMIDMmTmcC
[35] R. Chauvin, P.-H. Maire, B. Rebourcet, I. Bertron, Two-dimensional entropy-consistent collocated Lagrangian hydrodynamics methods for solving gas dynamics, in: MULTIMAT conference, Los Alamos National Laboratory, Sandia National Laboratories, 2017, santa Fe, NM, USA.
[36] S. Peluchon, G. Gallice, P.-H. Maire, Some acoustic-transport splitting schemes for two-phase compressible flows, in: ECCOMAS Congress,

2016.
[37] E. Tadmor, Entropy stability theory for difference approximations of nonlinear conservation laws and related time-dependent problems, Acta Numerica 12 (2003) 451–512.
[38] ParaView, https://www.paraview.org/, (Last accessed 29th May 2018).